

Illumination and turbidity effects on observing faceted bottom elements with uniform Lambertian albedos

Kendall L. Carder,¹ Cheng-Chien Liu,² Zhongping Lee, David C. English, James Patten, F. Robert Chen, and James E. Ivey

College of Marine Science, University of South Florida, 140 7th Avenue South, St. Petersburg, Florida 33701

Curtiss O. Davis

Naval Research Laboratory, Code 7212, Washington, D.C. 20375

Abstract

Aircraft images were collected near Lee Stocking Island (LSI), Bahamas, with wavelike features for bright sand bottoms during times when solar zenith angles were large. The image contrast between leading and trailing wave facets approached a 10–15% difference because of algae accumulations in wave troughs or topographic variations of the bottom. Reflectance contrast for blue light was greater than for red and green wavelengths when algae or detritus was present in the troughs. However, the contrast at green and red wavelengths was greater than at blue wavelengths when caused by the interplay between bottom topography and oblique illumination. A three-dimensional backwards Monte Carlo (BMC) model was developed to evaluate the effect of oblique illumination on wavelike topographic features for various values of water clarity and bottom albedo. An inverse optical modeling approach, previously developed for flat, horizontally homogeneous bottoms, was applied to the BMC results. Bathymetric estimates for bright facets tilted 10° toward the sun were slightly smaller than actual depths, whereas shaded facet depth estimates were too high by about 5%. Larger errors were associated with albedo retrievals, where shaded facets produced albedo estimates up to 15% lower than actual values. Errors increased with tilt angles up to 20° but decreased with sea and sky turbidity. Averaging sunlit and shaded pixels before running the inverse model reduced the uncertainty of bathymetric and albedo estimates to about 2 and 5%, respectively, comparable to previous field evaluations of the inversion model.

During the latter half of May and the beginning of June in 1998, 1999, and 2000, the Coastal Benthic Optical Properties (CoBOP) study occurred in the waters adjacent to Lee Stocking Island (LSI), Bahamas. One of the goals of this study was to provide improved measurements and understanding of the effect of different bottom types on remotely sensed observations. Remote (aircraft, satellite, shipboard) and in situ observations of the water and bottom were made over spatial scales that ranged from a few centimeters to kilometers. As part of the interpretation of hyperspectral imagery from the airborne Portable Hyperspectral Imager for Low-Light Spectroscopy (PHILLS) sensor (Davis et al. 2002), we have examined the contribution of sloping or wave-scalloped bottoms (Carder et al. 2001) on upwelling

radiance under varying conditions of illumination and turbidity.

Recent works by Lee et al. (1999, 2001) demonstrate the utility of hyperspectral radiance data collected from above the sea surface for determining the inherent optical properties and chlorophyll concentrations of the water column, even for shallow waters. This inversion method (Lee et al. 1999) provides estimates of bottom depth and albedo if the assumption is made that the bottom is horizontal with a Lambertian bidirectional reflectance distribution function (BRDF), so that reflected radiance is independent of the incident and observational angles. For shallow waters in Tampa Bay (<5 m depth), bathymetric estimates accurate to within about 10% of measured depths were retrieved, except for regions where the bottom sloped significantly or the bottom-reflected radiance was less than 15% of the total measured radiance (Lee et al. 2001).

Zaneveld and Boss (2003) present a two-dimensional analytical model of upwelling radiance over a corrugated bottom to examine the combination of bottom morphology and reflectance. Although their model does not include skylight or absorption and scattering within the water column, it does explain some of the differences between bottom reflectance and the far field reflectance when the measurement is made several meters off the bottom.

Mobley et al. (2003) show that for level, ooid sand bottoms with illumination and viewing geometries consistent with PHILLS aircraft observations at LSI, the BRDF is essentially Lambertian, varying only about 4% from a constant value for depths greater than 3 m and water clarities as ob-

¹ Corresponding author (kcarder@monty.marine.usf.edu).

² Present address: NASA, Earth Science Application Directorate, Stennis Space Center, Mississippi 39529

Acknowledgments

Financial support was provided by the Office of Naval Research, Environmental Optics Program, and with the following grants and contracts: Office of Naval Research through N00014-96-1-5013, N00014-97-1-0006; the NRL Core program; and National Aeronautics and Space Administration through NAS5-31716. We thank Charles Mazel for the efficient and thoughtful guidance that he provided the research teams during the field expeditions, and we thank the captain and crew of the R/V *Suncoaster* for their support and advice. Thanks to Jeffrey Bowles, Megan Carney, and Mary Kappus and to the crew of the Bosch Aerospace AN-2 for the collection of the PHILLS data, and to T. Valerie Downes and Robert Leathers for processing the PHILLS data.

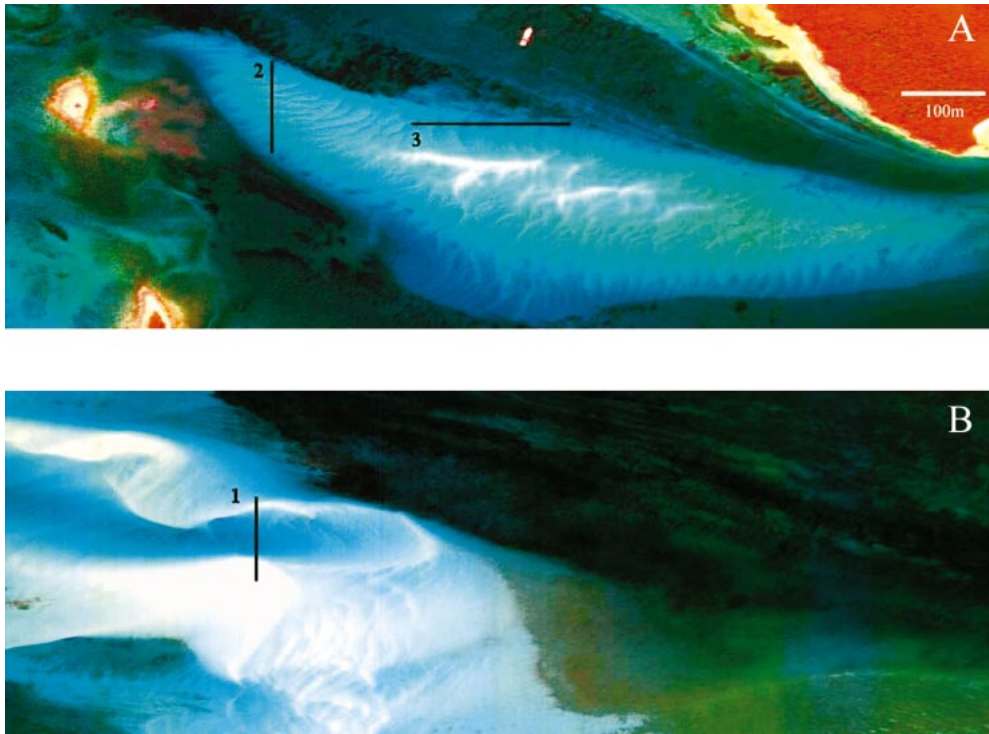


Fig. 1. PHILLS images of (A) Adderly Cut northwest of Lee Stocking Island and (B) a region west of Norman's Pond Key at about 0915 h EDT on 17 May 2000. RGB bands: 663, 551, 468 nm. Transect 1 crosses a large, shallow sand wave feature along the solar plane. Transects 2 and 3 cross sand waves along and orthogonal to the solar plane, respectively.

served near LSI. Thus, the Lambertian BRDF assumption of the Lee method is appropriate for PHILLS observations of these sandy areas. Mobley and Sundman (2003) also demonstrate that a one-dimensional radiative transfer model with a simple correction factor ($1D \times CF$) for solar photons can predict upwelling radiance values with better than 5% accuracy for flat, gently sloping bottoms ($<10^\circ$ incline). Their model can be used for comparisons with backwards Monte Carlo (BMC) modeled radiance reflected from a corrugated, sawtooth patterned bottom as a model validation step.

Because the depth gradient of a bottom can be estimated by applying the Lee inversion method to hyperspectral aircraft imagery, a Mobley and Sundman (2003) correction factor combined with the Lee inversion method should improve accuracy of subsequent bottom albedo estimates. The Mobley correction is not, however, applicable when the bottom is not flat and gently sloping or when the bottom is corrugated within the area viewed by an aircraft or spacecraft pixel. One goal of this paper is to ascertain the accuracy of water depth and bottom albedo estimates from the Lee et al. (2001) inversion method for corrugated bottoms in shallow water.

Bottom reflectance, water depth, optical absorption and scattering all contribute to the variability observed in scenes of remotely sensed radiance. PHILLS aircraft imagery collected during the CoBOP study at LSI show repeating wavelike and irregular bottom scour features (e.g., Fig. 1). One explanation for the wavelike patterns might be the focusing of sunlight on the bottom by surface waves, as discussed by

Zaneveld et al. (2001). However, most of the wavelike patterns apparent in the PHILLS imagery have wavelengths >5 m, which is inconsistent with surface waves generated in a shallow, short-fetch region. For that reason, many of the wavelike patterns of Figs. 1 and 2 are thought to be caused by sand waves, and the presence of these bedform structures was confirmed by diver observations and were documented with microtopographic images of the bottom measured by the Real-time Ocean-Bottom Optical Topographer (ROBOT, e.g., Fig. 3).

In addition to the PHILLS and ROBOT data, a variety of in situ optical measurements of the water column and bottom were collected near LSI. Although the spatial resolution of PHILLS was about 1.25 m, the resolution of the ROBOT sensor was several centimeters. In situ vertical profiles of optical properties could consist of a series of centimeter-scale measurements; however, these profiles or ship-based measurements of remote sensing reflectance might have been collected kilometers apart. A three-dimensional BMC model has been developed to combine these observations in a numerical simulation to determine the effects of bottom topography on depth and albedo estimates using hyperspectral aircraft data. This model is used to determine whether the high contrast of the wavelike patterns is due to bottom albedo differences (e.g., heavy minerals, algae, or detritus more concentrated in the troughs than on the crests) or unequal illumination (e.g., shadow effects) of sand waves.

The radiances computed by the BMC model over a uniform horizontal bottom are comparable to radiances pre-

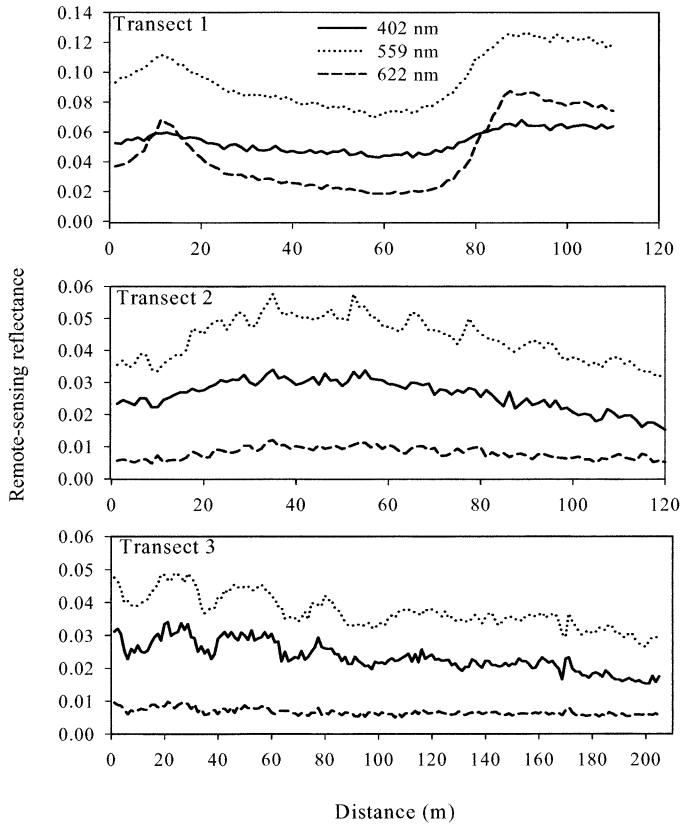


Fig. 2. PHILLS remote sensing reflectance transects at channels 402, 559, and 622 nm over sand wave and algal features from Fig. 1 (Transect 1 from Fig. 1B; Transects 2, 3 from Fig. 1A).

dicted using Mobley's (1994) Hydrolight model. The BMC model was also initiated with a predominantly oblique light field, fixed average water depth, and a corrugated bottom of uniform albedo to mimic the environment viewed by the PHILLS sensor. The resulting modeled upwelling radiances from the illuminated, shaded, or composite bottom slopes were then used as surrogate spectral radiances for the Lee reflectance inversion method. The resulting estimates of depth and albedo were compared to the original values to evaluate the accuracy of the Lee inversion method when used over shallow, corrugated bottom types. The BMC model was also executed using a sinusoidal bottom shape for comparison to the corrugated and flat bottoms.

Data

Various bottom types are present in the LSI region, including ooid sand, coral sand, seagrass, algal mats, and benthic diatoms. Most sand albedos or bottom reflectance values at LSI ranged between 0.2 and 0.6, whereas for areas with concentrations of either detritus or algae, the reported albedos were lower.

PHILLS is a hyperspectral sensor that was flown over LSI during the CoBOP field program at about 3,000 m altitude, providing a spatial pixel resolution of about 1.25 m (Davis et al. 2002). PHILLS was flown when the solar zenith angles were in the range of 40–60° in order to avoid sun glint

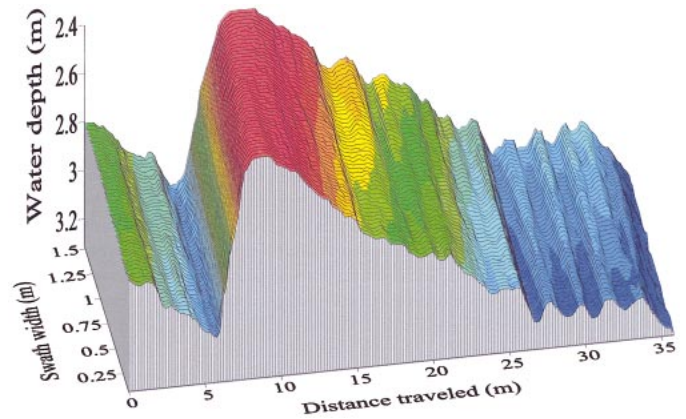


Fig. 3. Three-dimensional bathymetry collected from the RO-BOT on 21 May 1999 over an ooid sand shoal near Adderly Cut. Large waves have a sawtooth pattern, whereas smaller waves are more regular, as on the right.

reflected from the sea surface. Hence, according to Snell's Law, the subsurface solar illumination was directed from about 32–40° from the vertical. Spectral images collected by PHILLS over the LSI waters include areas with contrasting spatial structures, which appear to be caused by oblique lighting of sand waves on the bottom (Fig. 1). Contrast is the ratio between the difference and the average of radiance from two adjacent areas. In addition to the contrast caused by differing illumination of sloping wave facets, detritus and algae with their smaller albedos were sometimes found on the lee sides or troughs of sand waves, modifying the contrast in a different way. Thus, images from airborne sensors such as PHILLS provide a measure of the effects on water-leaving radiance because of variability in both the topography and albedos of sand bottoms for the LSI study site.

Transects extracted from an example PHILLS image (Fig. 1) reveal some scour patterns (Fig. 2, Transect 1) and wave-like features (Fig. 2, Transects 2, 3). Bottom wave facets, shaded or tilting away from direct sunlight, appear not only darker but more bluish in color than the more directly illuminated facets. For example, Transect 1 is in a very shallow region and the blue light contrast between facets was smaller than that for green or red light, probably because of the reduction of direct yellowish solar illumination for facets tilted away from the sun. These shaded facets, however, are still fully illuminated by diffuse blue skylight. Transect 2 exhibits a similar reduction in the image contrast at blue wavelengths.

An increase in the contrast exhibited in imagery of sand waves can also be caused by the propensity for algae to grow on the more quiescent, lee sides of sand waves in high-current areas or by dark, heavy minerals located in the troughs of sand waves (Fig. 1; Fig. 2, Transect 3). In these instances, the contrast is similar for blue wavelengths if not greater than for green wavelengths. This would be expected because algae absorb blue light more completely than green light. The contrast viewed in Transect 3 is more an effect of true albedo differences than of interactions between illumination geometry and topographic features because the solar

plane is parallel to the wave crests, equalizing the solar radiance incident on both sides of the crest of a sand wave.

For clean waters and clear skies, scattered light near the bottom is expected to be predominantly blue because of the inverse-wavelength (λ^{-4}) behavior of Rayleigh scattering of the sky and water molecules and the reduced absorption of pure water at blue wavelengths relative to longer wavelengths (Pope and Fry 1997). This increases the apparent blue reflectivity of indirectly illuminated bottoms because this scattered light is similarly reflected from both sides of a wave, whereas yellow-rich, direct solar light is reduced on the shaded sides of sand waves. However, heavy minerals and algae absorb as much or more light at 440 nm as at 550 nm. The blue-rich reflectance spectra for many of the dark areas of wavelike bottom patterns for the imagery implies that such periodic contrast variations were not caused by increased concentrations of benthic diatoms or minerals in the troughs of the waves and that a quantitative evaluation is needed of oblique illumination effects on a rough bottom.

The topographic structure representative of the bottom at LSI is required to parameterize models of the light field. The ROBOT is a range-measuring system consisting of a laser fan beam projected onto the bottom and viewed obliquely by a frame-processing camera as described in Carder et al. (2001). It was mounted on an Ocean Explorer-class autonomous underwater vehicle provided by Florida Atlantic University (Smith et al. 1995) and nominally operated 2 to 3 m above the bottom, providing a bathymetric swath approximately 1.5 to 2 m wide.

Some bedforms typical of the ooid sand region northwest of LSI (bright area containing Transects 2 and 3, Fig. 1A) are presented in Fig. 3 as measured by the ROBOT. The water depth in this area is about 4 m, and sand waves here appear to be long-crested. The ROBOT transect shows maximum bottom slope angles of $<17^\circ$, with wavelengths of the sand features ranging up to 20 m. Note that the form of large bottom features might not be sinusoidal, but sawtoothed in shape, whereas the small wavelike features are more sinusoidal.

Discrete water samples and apparent and inherent optical properties were measured in the waters surrounding LSI. The BMC model used chlorophyll concentration as an input parameter, with all optical properties covarying with it as in Morel (1988). Chlorophyll *a* (Chl *a*) concentrations measured in the waters immediately adjacent to LSI ranged from 0.10 to 0.16 mg m^{-3} , with an average value about 0.14 mg m^{-3} . We evaluate turbidity effects on the contrast between brightly and dimly illuminated facets of sand waves due to illumination geometry by varying Chl *a* concentrations from 0.01 to 0.5 mg m^{-3} , a larger range than observed at LSI, in order to more completely evaluate turbidity effects.

Models

Mobley et al. (2003) discusses the necessity of using a three-dimensional radiance transfer (RT) model instead of a general one-dimensional (1D) RT model, such as his Hydrolight model, to deal with the problem of nonuniform bottoms. They also discuss a simple correction factor (1D \times

CF) that increases Hydrolight's predictive accuracy for cases with sloping bottoms. They conclude that, for a bottom slope angle $\theta_b < 10^\circ$, a 1D RT model, used with the 1D \times CF correction factor, can predict the nadir-viewed radiance L_u with less than 5% uncertainty for solar photons. For the case of a corrugated bottom in shallow water, however, the reflected radiance between adjacent bottom facets plays a significant role in L_u , as do internal reflections from the sea surface and diffuse skylight. This study attempts to explore the limitations of using the Mobley 1D \times CF approach to predict the contrast caused by the sandy, corrugated bottoms when sunlight and skylight are both included. We compare the Mobley 1D \times CF results for a flat, tilted bottom of 10° with BMC results for sawtooth-patterned sand waves of similar slope angles to explore the limitations of the 1D \times CF approach.

A simplified shallow-water bottom with sand waves and the associated coordinates are illustrated in Fig. 4A. The corrugated bottom is modeled as continuous wavelike ramps repeating in the *x*-direction and labeled as Ramp₋₂, Ramp₋₁, Ramp₀, Ramp₁, and Ramp₂. Each simplified wave is long-crested and orthogonal to the solar plane (*x*-axis). Because the horizontal variance of radiance incident on the sea surface is negligible, we can focus on a single ramp, Ramp₀, and assume that it is bounded by two virtual walls, as shown in Fig. 4B. If a photon escapes through one wall at coordinate (*x*, *y*, *z*), another photon traveling in the same direction can be supplied immediately to the same position ($-x$, *y*, *z*) on the opposite wall to retain the photon in the calculation cell. The optical pathway *e* in Fig. 4B provides an example. This assumption does not change the computational cost of the model. It is, however, convenient for the program code. Figure 4B also illustrates the optical pathways that contribute to the sensor-detected radiance and the geometric specifications of the bottom.

The BMC model is an extension of the work of Liu (2000). Using radiance reciprocity arguments (Gordon 1985), a beam of light is simulated by a very large number (bundle) of photons emitted from the sensor to the waterbody (backwards). A set of bio-optical models, as used in Hydrolight, is employed to parameterize the inherent optical properties (IOPs) as a function of the Chl *a* concentration, with the water column assumed to be homogeneous (Case 1 waters). The path length before a photon hits another particle is a function of the beam attenuation coefficient (Gordon 1994). Once a collision occurs, the intensity of the photon bundle is attenuated by multiplying by the single-scattering albedo. The direction of bundle travel is modified by scattering and the ray tracing is continued. The polar scattering angles relative to the photon direction are determined by the normalized volume scattering phase function (Mobley 1994), and the azimuthal scattering angles are randomly distributed (Gordon 1994). Note that the scattering contribution from pure water is calculated analytically, whereas the contribution from particulate matter is specified by the averaged particle phase function (Mobley 1994). If the photon hits the bottom before it hits another particle, the position of intersection, as well as the bottom slope, is recorded. The bottom is assumed to have a Lambertian distribution of reflected radiance with a bottom albedo or irradiance reflectance, ρ_b .

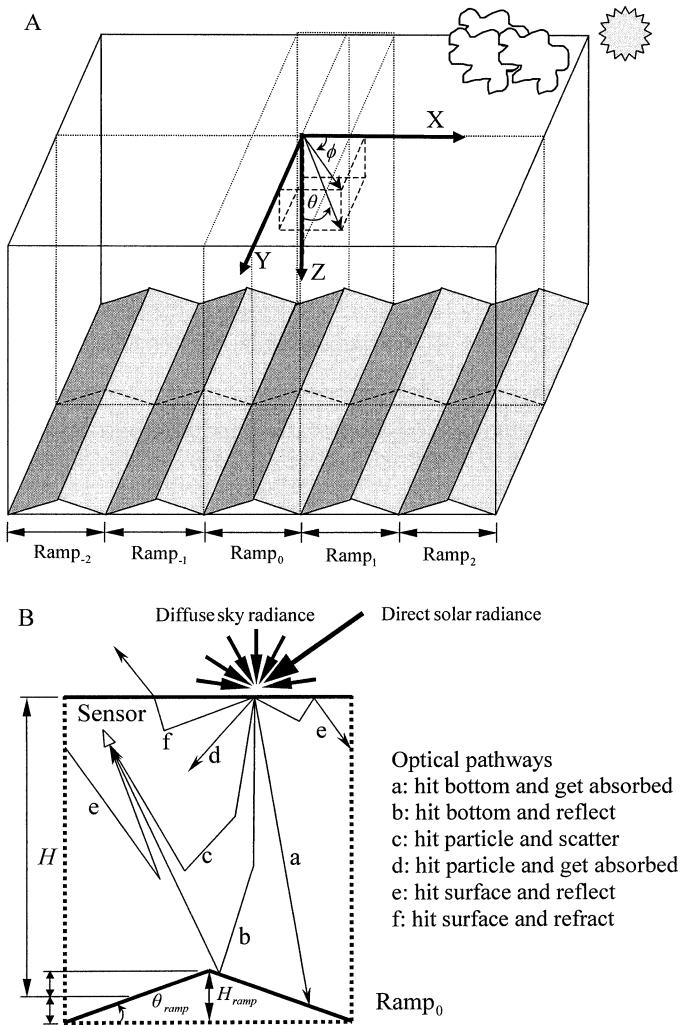


Fig. 4. (A) Representation of a shallow bottom with sand waves and the associated coordinates, with θ defined as the nadir angle and ϕ as the azimuth angle and with the x -axis directed toward the sun. (B) Illustration of optical pathways that contribute to the sensor-detected radiance and the geometric specification of bottom. H is the mean depth of the water column, H_{ramp} is the height of the ramp, and θ_{ramp} is the elevation angle of the ramp from the horizontal. Symmetry allows photons leaving the right wall to re-enter the same volume on the left (ray e).

Therefore, the photon will be reflected from the position of intersection into any direction of the hemisphere above the local bottom facet, and its intensity is attenuated according to the irradiance reflectance, ρ_b (Mobley 1994). Ray tracing continues, with special attention paid to whether the photon hits an adjacent bottom facet before it hits another particle or the air–sea interface. The sea surface is assumed flat. If the photon hits the air–sea interface, Fresnel’s formula and the laws of geometrical optics (Mobley 1994) are used to determine the photon’s fate. If the photon is refracted through the air–sea surface, the remaining intensity, as well as its direction, is registered. If the photon is reflected from the air–sea surface, ray tracing is continued.

Above-surface solar irradiance was simulated by the model of Gregg and Carder (1990), and the sky radiance distri-

bution was calculated using the model of Harrison and Coombes (1988). The default atmospheric visibility was set to 15 km. The BMC uses the same sky radiance model as Hydrolight (Mobley 1994) to allow direct comparison of the BMC and Hydrolight results. The sea surface is assumed flat, and the IOPs of the water column are assumed homogeneous. A set of bio-optical models for Case 1 waters, as used in Hydrolight, is employed to parameterize the IOPs as a function of the Chl a concentration. The bottom is assumed to have a Lambertian distribution of reflected radiance with a bottom albedo or irradiance reflectance, ρ_b . The geometry of the ramp is specified by the ramp angle, θ_{ramp} , and the ramp height, H_{ramp} . The radiance field can then be computed at any location in the water column for any viewing angle.

The hyperspectral inversion method (Lee et al. 1999, 2001) uses a priori assumptions about water column constituents. It iteratively varies water column constituents, depth, and bottom albedo until a best fit is obtained to the observed hyperspectral radiance shape. The model determines the length that a water column must be for a photon path (sea surface to bottom to surface) to filter the incident light enough to provide the color observed. Because of the strong absorption of water in the red wavelengths, if the color of water-leaving radiance is red-rich, the water column should be shallower than if the color is blue-rich.

Because the Lee inversion technique uses an optimization approach to best fit the measured remote sensing reflectance curves with model curves, minimizing error in one part of the spectrum can at times increase it elsewhere. The errors, then, do not necessarily scale monotonically with wave slope or sun angle. For the present study, the BMC model was constrained to six spectral channels. Usually the inverse model uses at least 18 spectral channels from 400 to 800 nm.

Results and discussion

BMC models are well suited to the task of evaluating two- or three-dimensional environmental simulations (Gordon 1985; Reinersman and Carder 1995; Reinersman et al. 1998; Mobley et al. 2003). The shape of recurring, long-crested sand waves can be approximated with simple ramp pairs, as shown in Fig. 4B.

For illustration, Fig. 5 shows the BMC model results for an optically clean, 10-m water column where the corrugated bottom has a ramp height of 0.8 m and $\pm 10^\circ$ slopes. The clean water is an extreme case because diffuse scattering is minimized along the path of a photon. Even so, the diffuse contributions from the sky and water paths are significant, as evidenced by the reduced 400-nm contrast between directly and indirectly illuminated wave facets. Note that results for $\pm 10^\circ$, tilted flat bottoms (Hydrolight with 1D \times CF; Mobley and Sundman 2003) where the total incoming irradiance to the sea surface is the same as for the BMC model case, nearly match the corrugated BMC results for individual facets at 560 nm. At 400 nm, however, the tilted, flat bottom provides greater contrast than the BMC corrugated results. The BMC predictions for a 10° corrugated bottom also produces significantly less contrast at 400 nm than

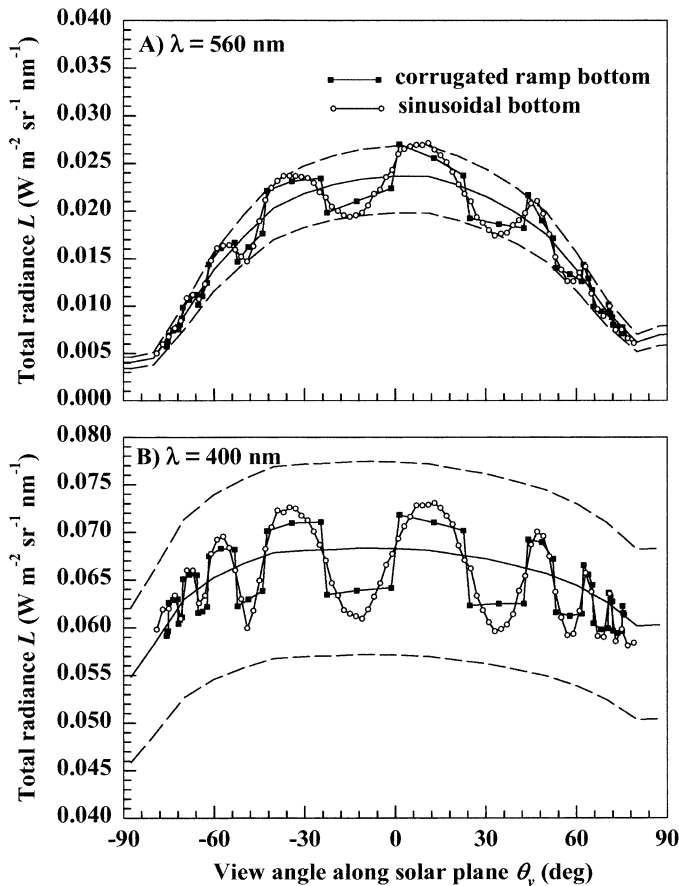


Fig. 5. (A) Green and (B) blue radiance modeled for the subsurface view above a sand wave crest (Fig. 4) with $H = 10$ m, $H_{\text{ramp}} = 0.8$ m, $\rho_b = 50\%$, and extremely clear water (see case I in Morel [1988]: $\text{Chl } a = 0.01 \text{ mg m}^{-3}$). The sand wave crests are oriented perpendicular to the solar plane, and the solar zenith angle is 60° . Solid squares are model results with corrugated ramp bottom; open circles are results for a sinusoidal bottom. Dashed lines are HydroLight results with correction factors for flat bottoms (solid line) sloped at 10° toward (upper line) and away (lower line) from the sun.

at 560 nm because of shadow infilling by diffuse (mostly Rayleigh) light. Recall that the $1D \times CF$ modification to HydroLight applies only to direct photons and does not include skylight, which represents 57% of the incoming light at 400 nm and 41% of the light at 560 nm. For a visibility factor of 50 km, these ratios become 42 and 20%, respectively, which would increase the contrast of the sand wave facets. The upwelling radiance can be shown to be maximal on the illuminated side of the corrugation crest, where the incidence angle equals the reflectance angle for rays hitting the bottom. With a solar zenith angle of 60° , the subsurface solar zenith angle is about 40° , so the bottom slope projecting the brightest return toward zenith is about 20° from horizontal.

Note in Fig. 5 that the 10° sawtooth pattern produces a smaller maximal reflected signal than does the sinusoidal pattern, which has a maximum bottom slope angle of 14.1° , which is closer to the brightest bottom slope angle of 20°

Table 1. List of the computational conditions used in the backwards Monte Carlo model for the purposes of understanding how the contrast is influenced by various factors. Each factor of the standard case is varied one at a time as the comparative case.

	Standard case	Comparative case
Solar zenith angle, θ_{sun} (degrees)	60	0, 30, 60
Depth of water column, H (m)	5	2, 5, 10
Chl a concentration (mg m^{-3})	0.01	0.01, 0.1, 0.5
Lambertian bottom reflectance, ρ_b	0.5	0.2, 0.5
Atmospheric visibility, V_i (km)	15	5, 15, 50
Ramp angle, θ_{ramp} (degrees)	10	10, 15, 20

than is 10° . BMC model simulations for bottom slope angles up to 20° are made in order to include angles providing maximal radiance from the bottom to a nadir-viewing aircraft sensor. From Fig. 5, it is clear that the effect of the water depth variation of 0.8 m (slope from viewing angle 0 – 24°) has a smaller effect on the upwelling radiance than has the bottom slope angle (slope from viewing angle $+0^\circ$ to -0°), especially at 400 nm. Note for the sawtooth sand waves, the crest versus trough values for the sunlit side (viewing angle 0 – 24° , Fig. 5) decrease because of a range increase from sun to bottom to sensor of roughly 1.9 m, including slant-path effects. The additional absorption at 560 nm along that path difference is about 12%, which is very close to the 13% decrease observed from 0 to 24° in Fig. 5. The shade effect, on the other hand, is easy to observe by comparing $L_w(0^+)$ to $L_w(0^-)$ because both are at the same depth. This decrease is about 17% at 560 nm, or nearly 50% larger than the depth effect for the sunlit facet.

The effect of depth difference due to sand waves has only a 3% effect at 400 nm because of the small absorption coefficient ($\sim 1\%$) for these clear waters. The shade effect is 11%, or about two thirds of the effect seen at 560 nm because of the shadow infilling by additional diffuse sky and water path radiance at blue wavelengths.

To understand how the contrast between adjacent wave facets is influenced by various factors, a series of simulations (six spectral radiances) were executed based on the computational conditions listed in Table 1. All factors of a standard case are varied one at a time for sand waves with a sawtooth pattern. A hypothetical sensor is placed above a corrugation crest, just below the air–water surface (depth $z = 0^-$), providing a nadir view (θ_v) of either the sunny ($\theta_v = 0^+$) or shady sides ($\theta_v = 0^-$) of the crest. The contrast is defined as the ratio between the difference and the average of radiance from both sides near the crest, as detected by the hypothetical sensor.

$$\text{contrast } (z = 0^-) \equiv \frac{|L(\theta_v = 0^+) - L(\theta_v = 0^-)|}{0.5[L(\theta_v = 0^-) + L(\theta_v = 0^+)]} \quad (1)$$

Spectral contrast changes due to environmental variability—Figure 6A shows that the solar angle significantly affects the contrast of illuminated versus shaded sides of 10° corrugations. Note that with the sun at zenith, the corruga-

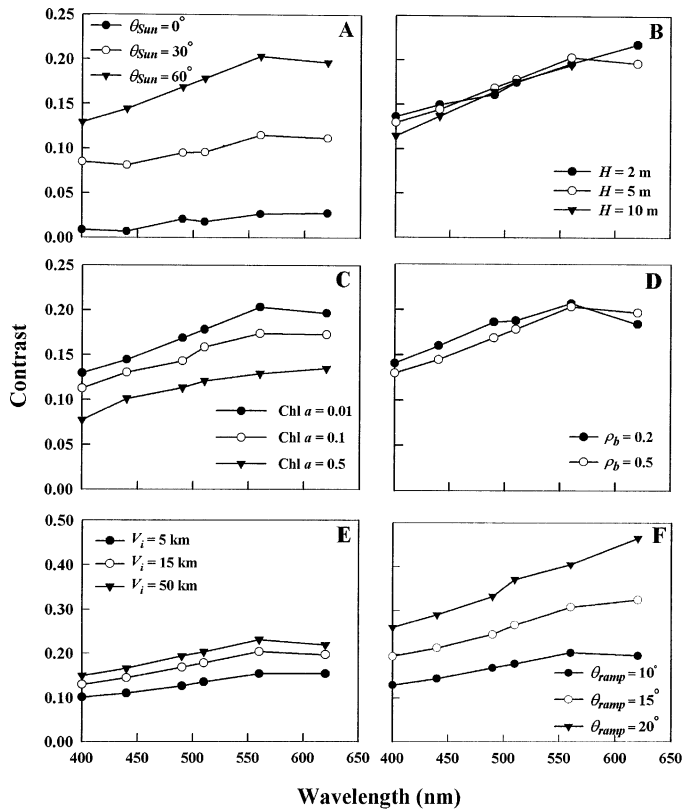


Fig. 6. Spectral contrast variations for sawtooth sand waves with environmental conditions listed in Table 1. Effects due to (A) solar zenith angle, θ_{Sun} ; (B) water column depth, H ; (C) Chl a concentration and covarying IOPs; (D) bottom albedo, ρ_b ; (E) atmospheric visibility at 550 nm, V_i ; and (F) ramp angle of wave facets, θ_{ramp} .

tions would be difficult to discern because their contrast would be near zero.

For water less than 10 m deep, the effect of bottom depth on corrugation contrast is relatively minor (Fig. 6B). For deeper clear waters, however, the contrast decreases slightly, especially at the Rayleigh-rich blue wavelengths. This is because of the increase in diffuse molecular scattering arising from the longer light paths of deeper waters. Similarly, as water turbidity increases, contrast decreases. In this BMC model, increasing turbidity is caused by an increase in chlorophyll concentration (Fig. 6C).

Increasing the bottom albedo results in a slight decrease in contrast (Fig. 6D). This is because both the shaded and illuminated areas are subject to multiple scattering from the water column, to reflected radiance from an adjacent facet and to internal reflectance from the sea surface.

Decreasing the atmospheric visibility (transparency) from 50 to 5 km (Fig. 6E) makes the light field above the sea surface more diffuse. The BMC model predicts a reduction in contrast, as one would expect.

Increasing the facet slope of bottom corrugations where they are obliquely illuminated significantly increases the contrast (Fig. 6F). With the sun at a large solar zenith angle (60°) and shining through clear water and sky, the contrast between facets of sand waves can become as large as 45%

for bottom facet slopes of 20° . Recall that a nadir view of a bottom facet with a 20° slope toward the sun is optimal for maximal reflectance for subsurface illumination at a 40° solar zenith angle.

Spectral bathymetric and albedo retrievals—The radiances generated from the BMC simulations discussed above were subsequently used as inputs for the inversion method of Lee et al. (1999, 2001). This inversion of the Lee et al. (1998) remote sensing reflectance model provides estimates of water IOPs, water depth, and bottom albedo. Subsequently, these estimated depths and albedos are compared to the original values used by the BMC model. The estimates are not expected to exactly match the original values because the Lee inversion assumptions include a horizontal bottom, whereas the BMC model has produced near-nadir views of the illuminated and shaded bottom corrugations.

Table 2 presents errors in bathymetric and albedo estimates for the BMC simulations. Error percentages are presented as variations in the height of the water column, H , and bottom albedo, ρ , for the sunny and shady sides of the corrugation crests. These simulations were for long sand waves, (wavelength ≥ 10 m), as illustrated by the ROBOT data in Fig. 3. Errors for smaller sand waves with less vertical relief and slopes will be smaller. Also depicted in Table 2, Case 1, are the errors obtained if, before retrieving model inversion values, the illuminated and shaded BMC facets are averaged to simulate radiance data from a sensor with lower spatial resolution.

With clear water and a corrugated bottom, the Lee model underestimates water column depths for the sunlit facets and overestimates depths for shady ones. Most errors are less than 5%, except where slopes approach 20° . Averaging the contrasting radiances provides depths accurate to within 3% for all cases in Table 2, Case 1, even for slopes of 20° .

The error in the bottom albedo can reach 15% for shaded facets. However, except for very shallow water depths, accuracies improve to about 5% by averaging adjacent contrasting radiances.

Increasing water turbidity, depth, and bottom absorption all increase the relative contribution of the water-reflected photons relative to bottom-reflected photons, decreasing the influence of the bottom reflection on the above-water spectra. Increased water turbidity reduced the accuracy of albedo estimates for shaded facets; however, it increased bathymetric accuracies for both sides of a sand wave because diffuse light reduces the color distortions of the two facets from that of a horizontal bottom. Turbidity effects should not be dominant error sources for the PHILLS imagery evaluated here.

Table 2 also provides results for a hypothetical water type, where the light absorption by dissolved material is greater than that of chlorophyll at 440 nm (Case 2 waters). This is more representative of the water conditions for the Adderly Cut region near LSI than the conditions used in Table 2, Case 1. According to these results, bathymetry errors ca. $<3\%$ and albedo errors $<15\%$ can be attributed to 10° sand waves if the method of Lee et al. (2001) is applied to accurate spectral images of the Adderly Cut region. For spatially averaged data, including both sunny and shaded sides of the waves, the sand wave errors reduce to less than 1.4

Table 2. Error percentages of bathymetric and albedo retrievals for a wide variety of lighting and environmental conditions for long waves, such as illustrated by ROBOT data in Fig. 3. Case 1 waters, of which the IOPs are a function of the Chl *a* concentration [Chl *a*] based on a set of bio-optical models, are as used in Hydrolight. Gelbstoff-rich Case 2 waters have an extra CDOM component added. It only contributes to absorption and not to scattering. The absorption by CDOM is set to be 2.5 times that of the chlorophyll absorption at a reference wavelength of 440 nm.

θ_{Sun}	H	[Chl <i>a</i>]	θ_{ramp}	ρ_b	Error of bathymetric and albedo retrievals (%)					
					H_{shady}	H_{sunny}	H_{average}	ρ_{shady}	ρ_{sunny}	ρ_{average}
Case 1										
0					0.94	1.28	1.07	4.07	7.77	5.88
30	5	0.01	10	0.5	3.56	-1.58	0.77	1.38	6.76	4.00
60					5.86	-2.69	-0.16	-5.77	1.97	-2.39
60	2				6.05	-3.22	-0.94	-9.79	2.07	-3.50
	5	0.01	10	0.5	5.86	-2.69	-0.16	-5.77	1.97	-2.39
	10				5.74	-3.68	0.46	-2.32	3.29	1.10
60		0.01			5.86	-2.69	-0.16	-5.77	1.97	-2.39
	5	0.1	10	0.5	6.26	-1.44	2.89	-6.03	2.85	1.38
		0.5			1.35	-0.39	2.30	-12.00	0.53	-1.87
60			10		5.86	-2.69	-0.16	-5.77	1.97	-2.39
	5	0.01	15	0.5	9.02	-3.82	0.93	-10.03	4.54	-2.04
			20		11.78	-4.89	1.33	-15.60	3.87	-4.28
60	5	0.01	10	0.2	1.64	-4.18	-0.57	-13.49	0.54	-5.91
				0.5	5.86	-2.69	-0.16	-5.77	1.97	-2.39
Case 2										
60	2				-0.14	-2.50	-1.38	-15.29	2.25	-6.42
	5	0.1	10	0.2	1.03	-0.52	0.28	-12.22	3.98	-3.98
	10				-3.03	0.80	-0.94	-14.89	6.58	-4.27
60	2				2.20	-2.81	-0.42	-15.75	-2.88	-9.12
	5	0.1	10	0.5	-0.23	-0.91	0.48	-14.81	2.83	-3.62
	10				-2.05	-0.69	-1.17	-14.43	2.68	-5.55

and 9.1%, respectively. These errors would be in addition to those implicit in the inversion method (Lee et al. 1999). Increasing the wave slopes will increase the errors, but reducing the solar zenith angle will decrease the errors.

Lee et al. (1999) found that their estimates of depths averaged within 10% of the measured depths when using data from the Florida and the Bahamas shelves. For Tampa Bay in Florida (Lee et al. 2001), bathymetric accuracies averaged about 10–12%, except where the bottom slope was significant or the bottom signal contributed less than 15% to the water-leaving radiance. A slope of 20° inducing additional errors up to 12% in bathymetry and 16% in albedo for the shady sides of waves or sloping bottoms, as found in this study, is consistent with the field application of Lee et al. (2001).

PHILLS aircraft imagery of the shallow waters near LSI contain long-crested, wavelike bedforms that might have resulted from shading because of oblique illumination of sand waves or decreased albedo in the trough regions of the waves. The profiles of the reflectance patterns observed in the PHILLS imagery (Fig. 2 transects) are angular rather than smooth, suggesting the bottom waveform is sawtoothed rather than sinusoidal. The BMC model uses the assumption that the bottom is formed of repetitive symmetric ramps, whereas the actual bottom profiles measured with the ROBOT appear to be composed of asymmetric ramps.

With oblique illumination, the model provides shade effects consistent with patterns observed in PHILLS imagery along Transects 1 and 2. Notably, the contrast at blue wave-

lengths was lower than at longer wavelengths, and the contrast ranges were generally within the ranges observed in model results. When the BMC model was run with a 60° solar zenith angle, then ramp slopes as high as 20° and atmospheric visibilities as high as 50 km were required to approximate the reflectance contrast observed at blue wavelengths along Transect 1. However, PHILLS flew when the solar zenith angle was 52°, so the BMC overestimate of contrast for this PHILLS image is plausible. The observed contrasts of red and green reflectance were much larger than predicted by the BMC model, however, so the height of the sand waves might be greater than the model-assumed height or the albedo of the troughs might be darker than those of the crests.

The profiles of Transect 3, however, are inconsistent with simple topographic forcing of the obliquely lit light field because the transect is normal to the solar plane, minimizing topographic effects, and because blue contrast features equal or exceed variations observed at green and red wavelengths. Variations in bottom albedo from algal accumulations in sand wave troughs would provide a logical explanation for these contrast variations.

Bottom slope effects on bathymetric and albedo retrievals can be minimized by making flight operations at smaller solar zenith angles (e.g., 40°) under conditions where sand wave crests run parallel with the solar principal plane. Furthermore, if the slope of the bottom can be inferred from sequential bathymetric retrievals across wave forms in an image, there is a fair chance that the slope illumination ef-

fects on the albedo of the bottom can be corrected, at least in part (e.g., Mobley and Sundman 2002). However, such a research effort is beyond the scope of this paper and is left for future consideration.

References

- CARDER, K. L., D. K. COSTELLO, L. C. LANGEBRAKE, W. HOU, J. T. PATTEN, AND E. A. KALTENBACHER. 2001. Real-time AUV data for command, control, and model inputs. *IEEE J. Ocean. Eng.* **26**: 742–751.
- DAVIS, C. O., AND OTHERS. 2002. Ocean PHILLS hyperspectral imager: Design, characterization, and calibration. *Opt. Express* **10**: 210–221.
- GORDON, H. R. 1985. Ship perturbation of irradiance measurements at sea. 1: Monte Carlo simulations. *Appl. Opt.* **24**: 4172–4182.
- . 1994. Modeling and simulating radiative transfer in the ocean, p. 3–39. *In* R. W. Spinrad, K. L. Carder, and M. J. Perry [eds.], *Ocean optics*. Oxford Univ. Press.
- GREGG, W. W., AND K. L. CARDER. 1990. A simple spectral solar irradiance model for cloudless maritime atmospheres. *Limnol. Oceanogr.* **35**: 1657–1675.
- HARRISON, A. W., AND C. A. COOMBES. 1988. An opaque cloud cover model of sky short wavelength radiance. *Solar Energy* **41**: 387–392.
- LEE, Z., K. L. CARDER, C. D. MOBLEY, R. G. STEWARD, AND J. S. PATCH. 1998. Hyperspectral remote sensing for shallow waters. I. A semianalytical model. *Appl. Opt.* **37**: 6329–6338.
- , ———, ———, ———, AND ———. 1999. Hyperspectral remote sensing for shallow waters. 2. Deriving bottom depths and water properties by optimization. *Appl. Opt.* **38**: 3831–3843.
- , ———, R. F. CHEN, AND T. G. PEACOCK. 2001. Properties of the water column and bottom derived from AVIRIS data. *J. Geophys. Res.* **106**: 11,639–11,651.
- LIU, C. C. 2000. Using SeaWiFS ocean colour data to test a plankton ecosystem model. Ph.D. thesis, Imperial College, University of London.
- MOBLEY, C. D. 1994. *Light and water*, 2nd ed. Academic.
- , AND L. SUNDMAN. 2003. Effects of optically shallow bottoms on water-leaving radiances: Inhomogeneous and sloping bottoms. *Limnol. Oceanogr.* **48**: 329–336.
- , H. ZHANG, AND K. J. VOSS. 2003. Effects of optically shallow bottoms on water-leaving radiances: Bidirectional reflectance distribution function effects. *Limnol. Oceanogr.* **48**: 337–345.
- MOREL, A. 1988. Optical modeling of the upper ocean in relation to its biogenous matter content (case 1 waters). *J. Geophys. Res.* **93**: 10,749–10,768.
- POPE, R., AND E. FRY. 1997. Absorption spectrum (380–700 nm) of pure waters: II. Integrating cavity measurements. *Appl. Opt.* **36**: 8710–8723.
- REINERSMAN, P. N., AND K. L. CARDER. 1995. Monte Carlo simulation of the atmospheric point-spread function with an application to correction for the adjacency effect. *Appl. Opt.* **34**: 4453–4471.
- , ———, AND F.-I.R. CHEN. 1998. Satellite-sensor calibration verification with the cloud-shadow method. *Appl. Opt.* **37**: 5541–5549.
- SMITH, S. M., K. HEEB, N. FROLUND, AND T. PANTELAKIS. 1995. The ocean explorer AUV: A modular platform for coastal oceanography. *Proceedings of the 9th International Symposium on Untethered Submersible Technology*, Druham, New Hampshire.
- ZANEVELD, J. R. V., AND E. BOSS. 2003. The influence of bottom morphology on reflectance: Theory and two-dimensional geometry model. *Limnol. Oceanogr.* **48**: 374–379.
- , ———, AND A. BARNARD. 2001. Influence of surface waves on measured and modeled irradiance profiles. *Appl. Opt.* **40**: 1442–1449.

Received: 1 October 2001

Amended: 18 July 2002

Accepted: 18 July 2002